

**Oxovanadium(IV) complexes of curcumin for cellular imaging and mitochondria
targeted photocytotoxicity**

Bhabatosh Banik,^a Kumar Somyajit,^b Ganesh Nagaraju,^{*b} and Akhil R. Chakravarty^{*a}

Supporting Information

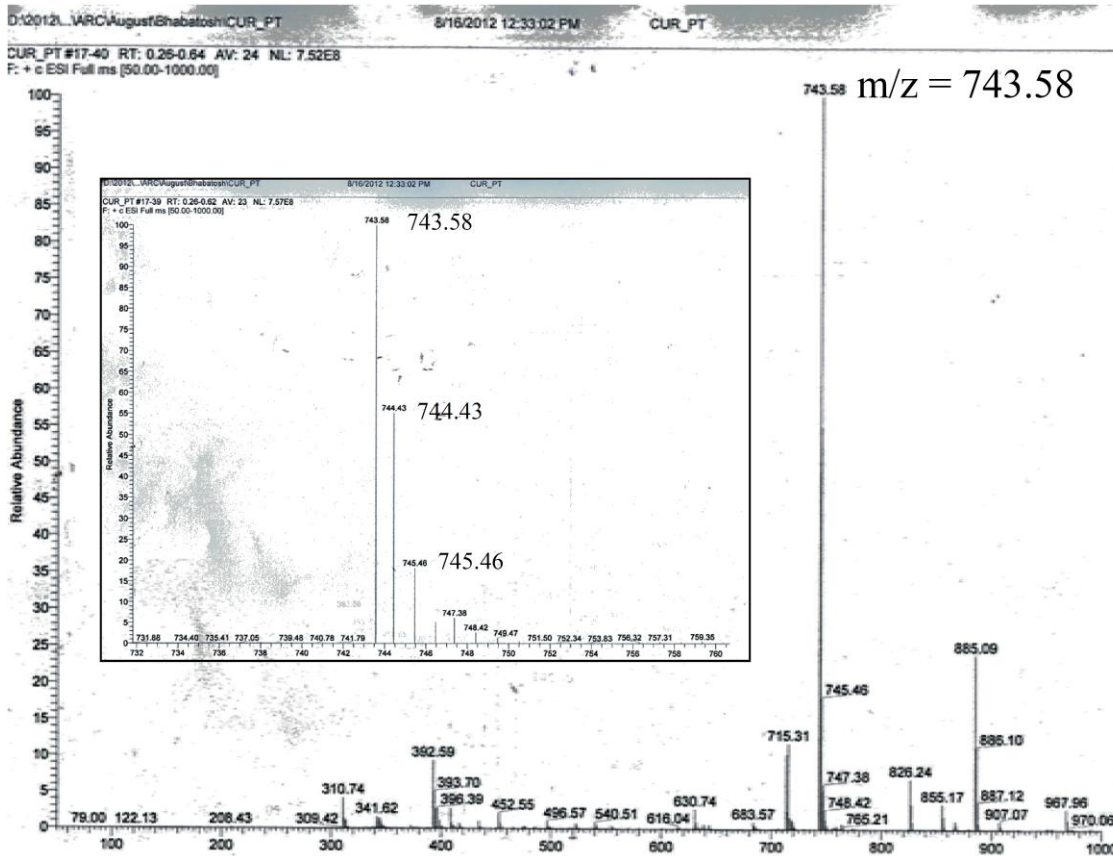


Fig. S1. The ESI-MS spectrum of complex **1** in MeCN showing the peak at 743.58 that corresponds to $[M - (ClO_4)]^+$. The inset shows the isotopic distribution of the $[M - (ClO_4)]^+$ ion peak.

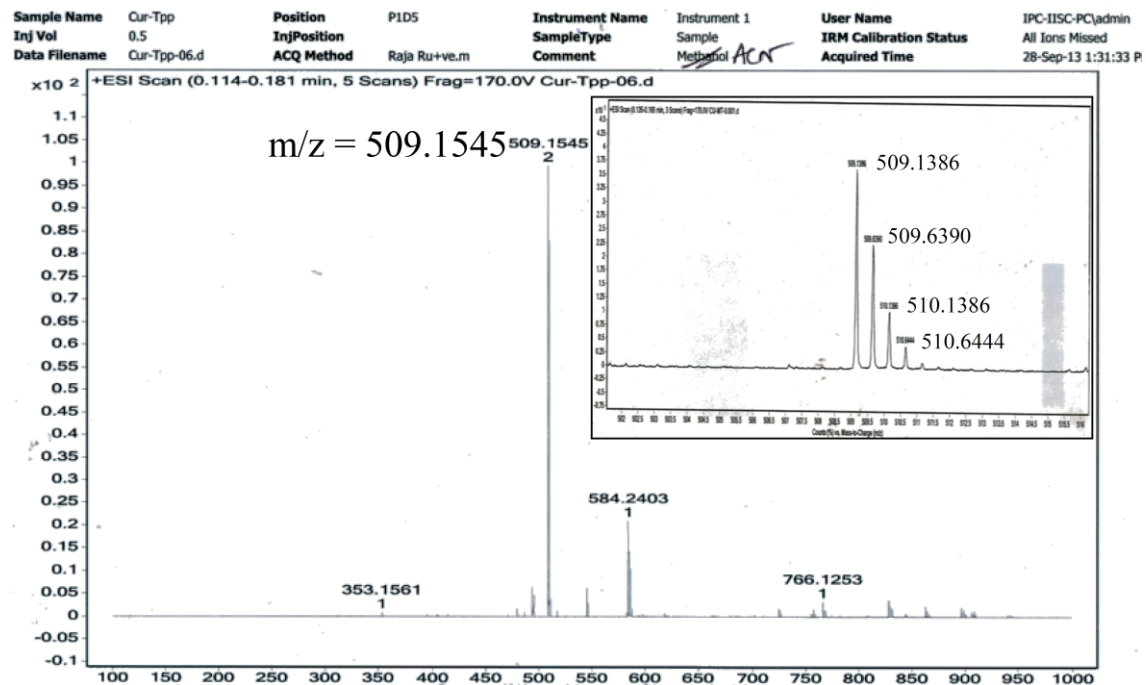


Fig. S2. The ESI-MS spectrum of complex **2** in MeCN showing the peak at 509.1545 (m/z) assignable to $[M - (\text{ClO}_4 + \text{Br})]^{2+}$. The inset shows the isotopic distribution of the $[M - (\text{ClO}_4 + \text{Br})]^{2+}$ ion peak.

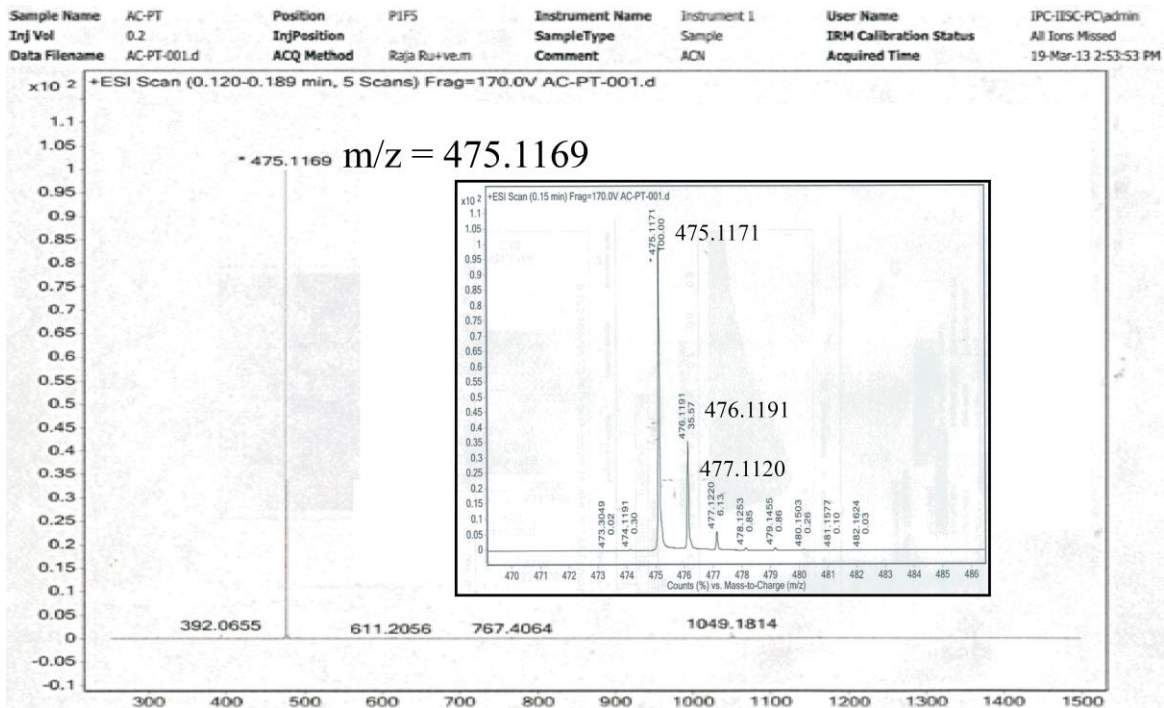


Fig. S3. The ESI-MS spectrum of complex **3** in MeCN showing the peak at 475.1169 that corresponds to $[M - (\text{ClO}_4)]^+$. The inset shows the isotopic distribution of the $[M - (\text{ClO}_4)]^+$ ion peak.

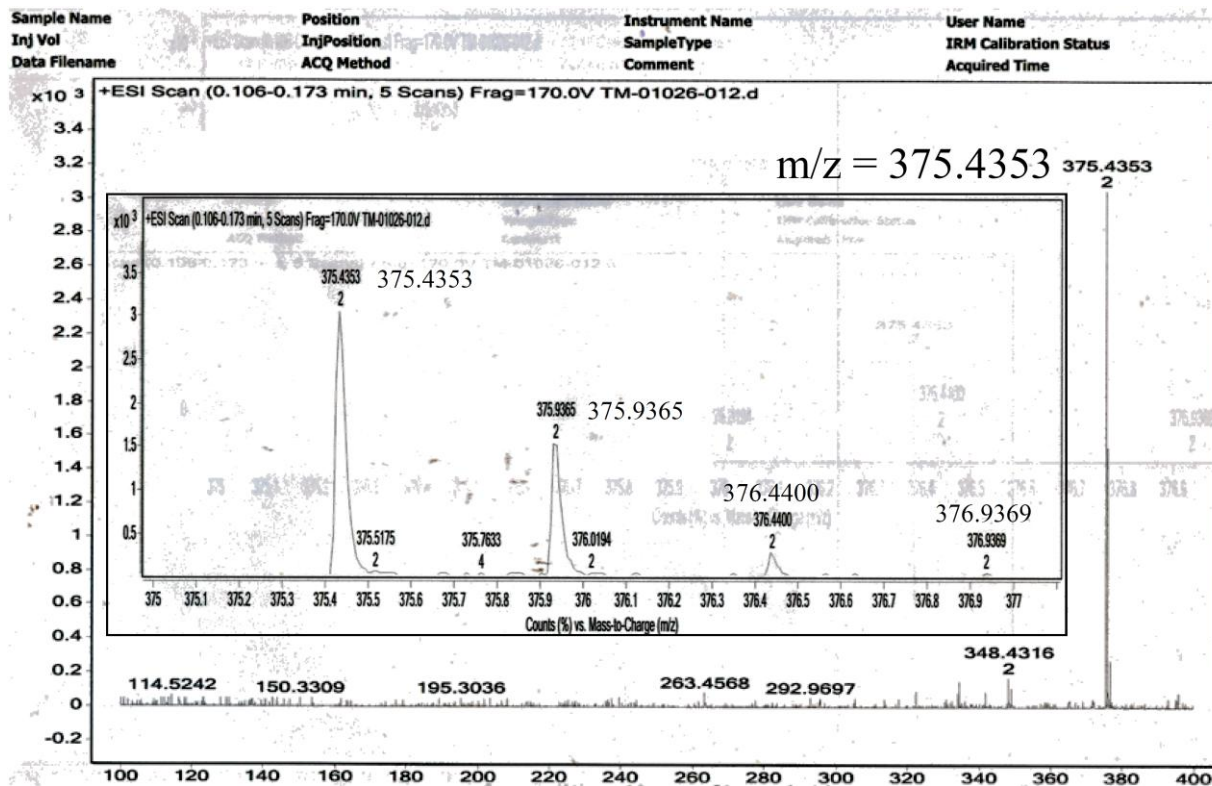


Fig. S4. The ESI-MS spectrum of the complex **4** in MeCN showing a peak at 375.4353 that corresponds to $[M - (\text{ClO}_4 + \text{Br})]^{2+}$. The inset shows the isotopic distribution of the $[M - (\text{ClO}_4 + \text{Br})]^{2+}$ ion peak.

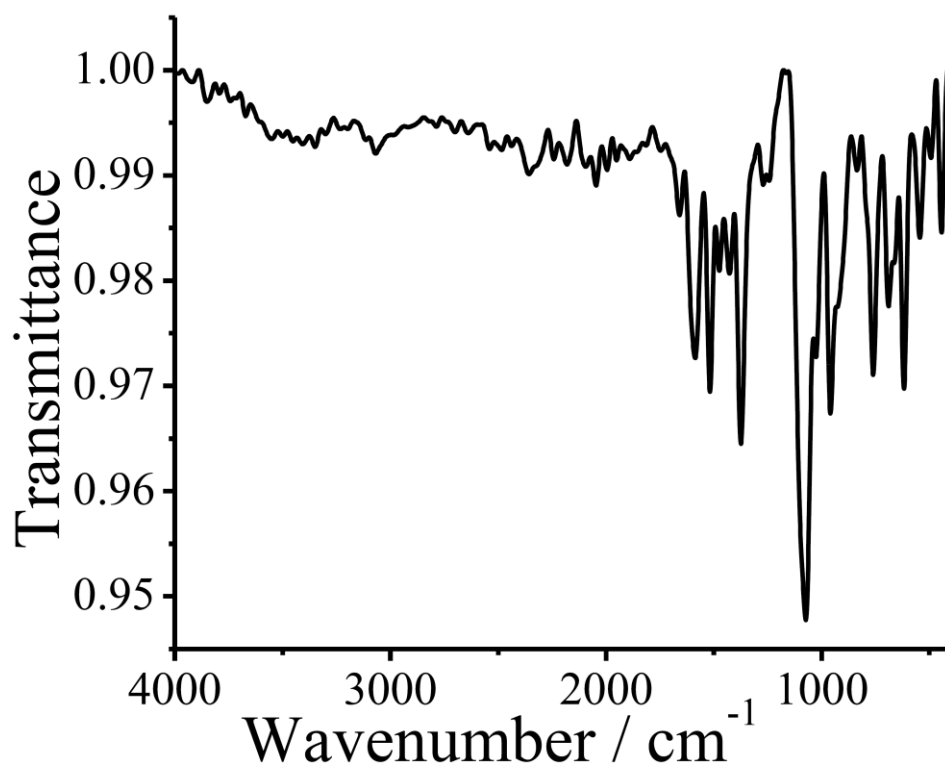


Fig. S5. IR spectrum of complex 1.

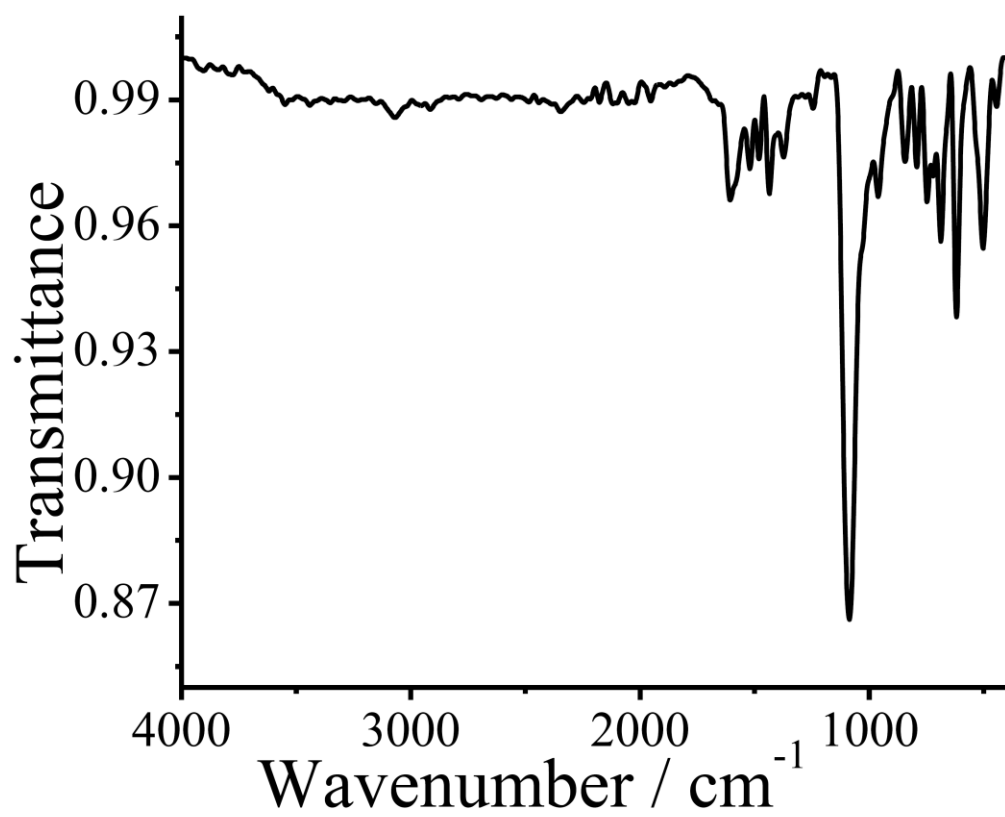


Fig. S6. IR spectrum of complex 2.

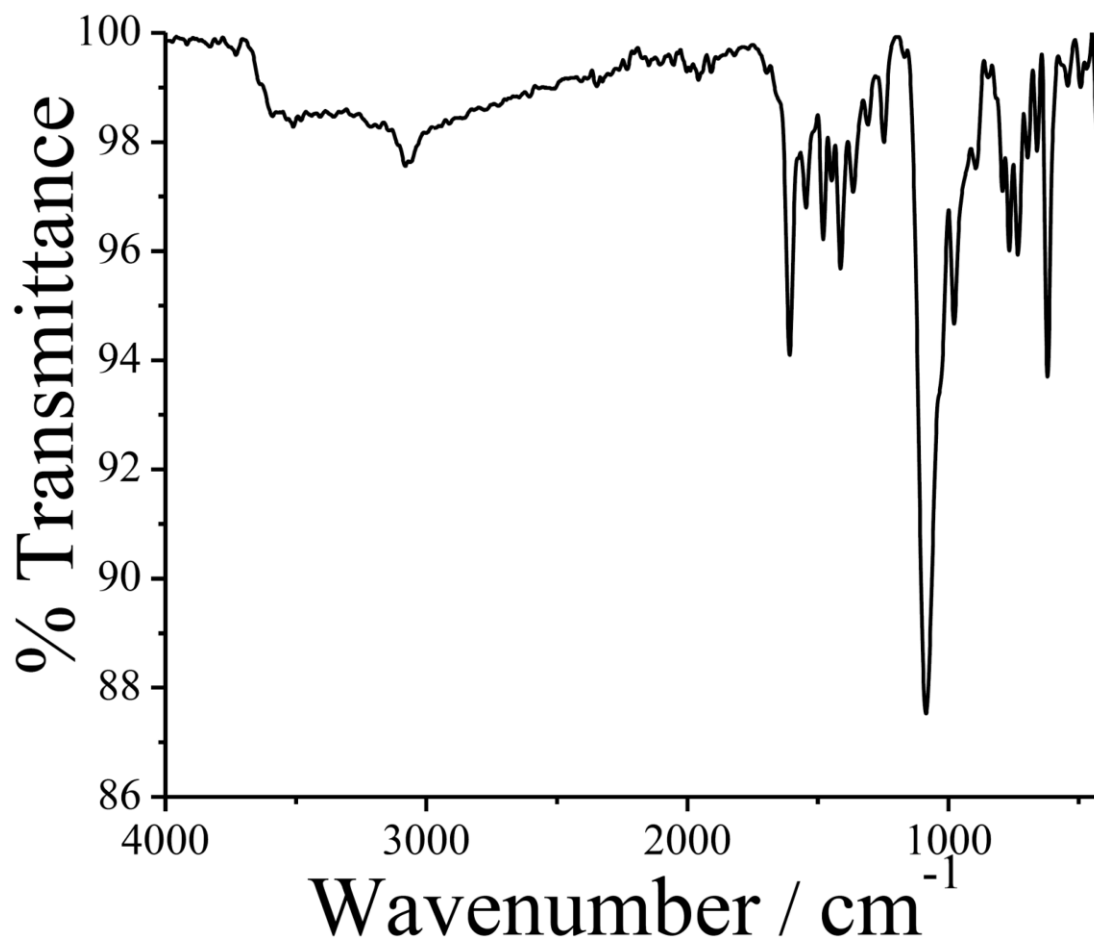


Fig. S7. IR spectrum of complex 3.

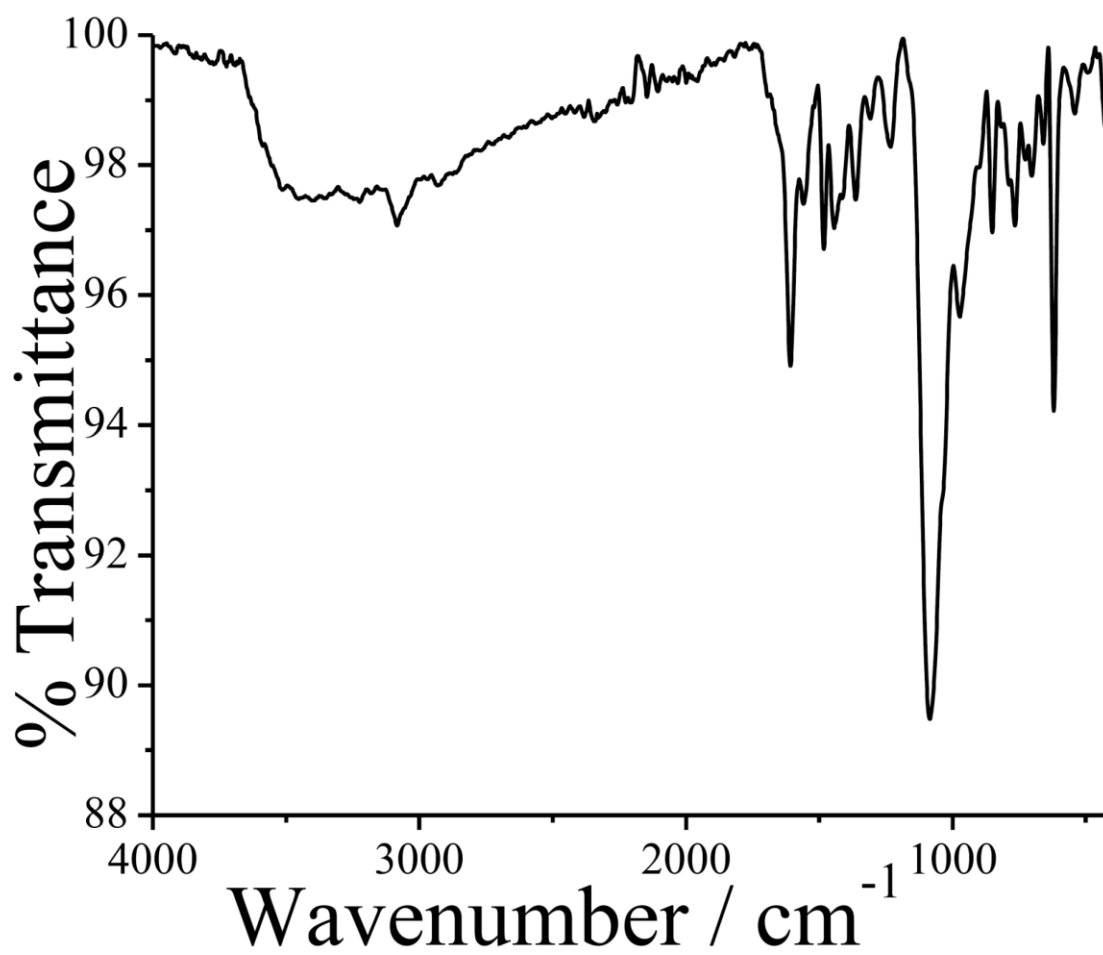


Fig. S8. IR spectrum of complex 4.

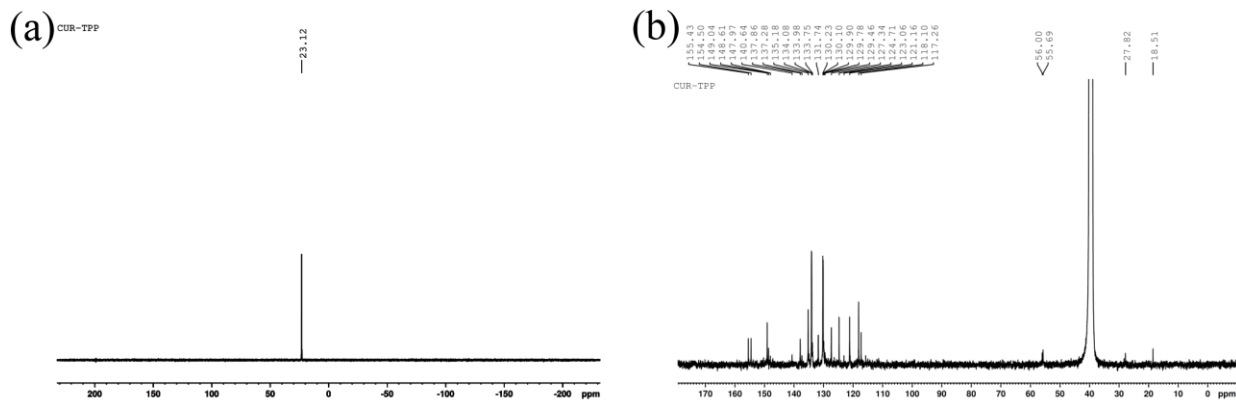


Fig. S9. (a) ³¹P NMR (162 MHz) of Complex **2** in DMSO-d₆: δ (ppm) 23.12. (b) ¹³C NMR (100 MHz) of Complex **2** in DMSO-d₆: δ (ppm) 155.43, 154.50, 149.04, 148.61, 147.97, 140.64, 137.86, 137.28, 135.18, 134.08, 133.98, 133.75, 131.74, 130.23, 130.10, 129.90, 129.78, 129.46, 127.34, 124.71, 123.06, 121.16, 118.10, 117.26, 56.00, 55.69, 27.82, 18.51.

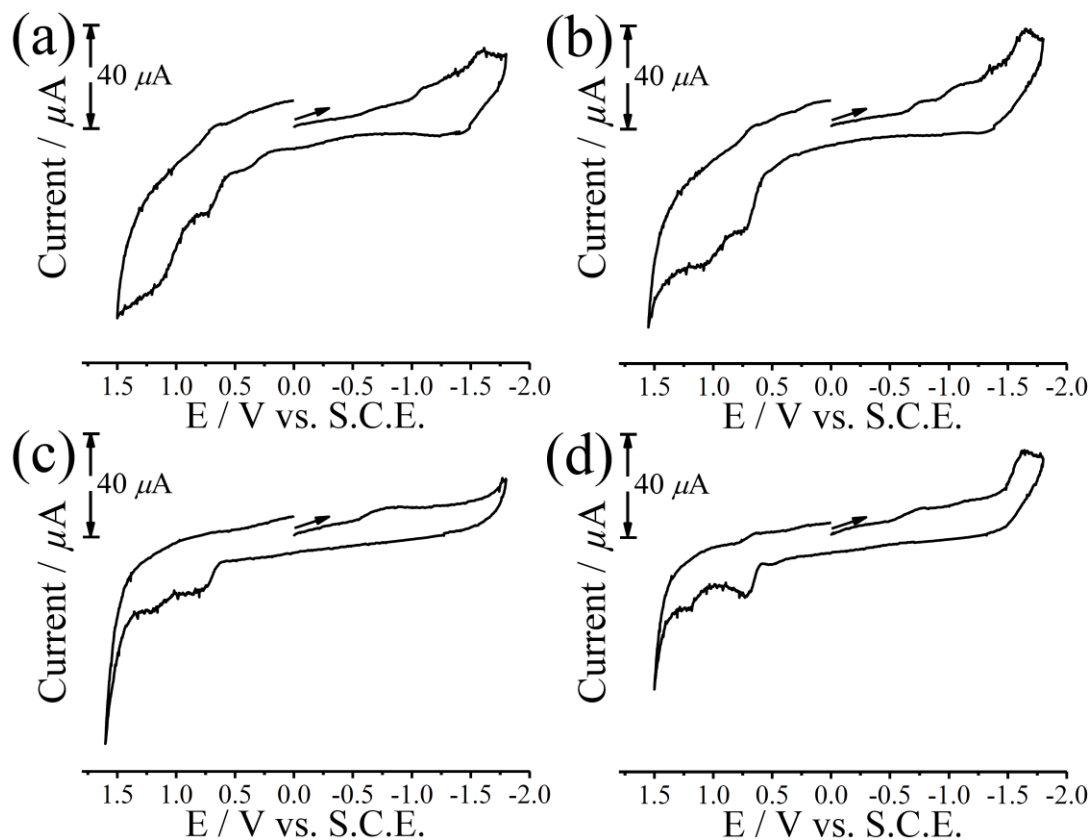


Fig. S10. Cyclic voltammograms of the complexes **1** (a), **2** (b), **3** (c) and **4** (d) in DMF at a scan rate of 50 mV s^{-1} and 0.1 M TBAP as the supporting electrolyte. The voltammetric responses are irreversible in nature showing only the cathodic or anodic peak without having any counterpart.

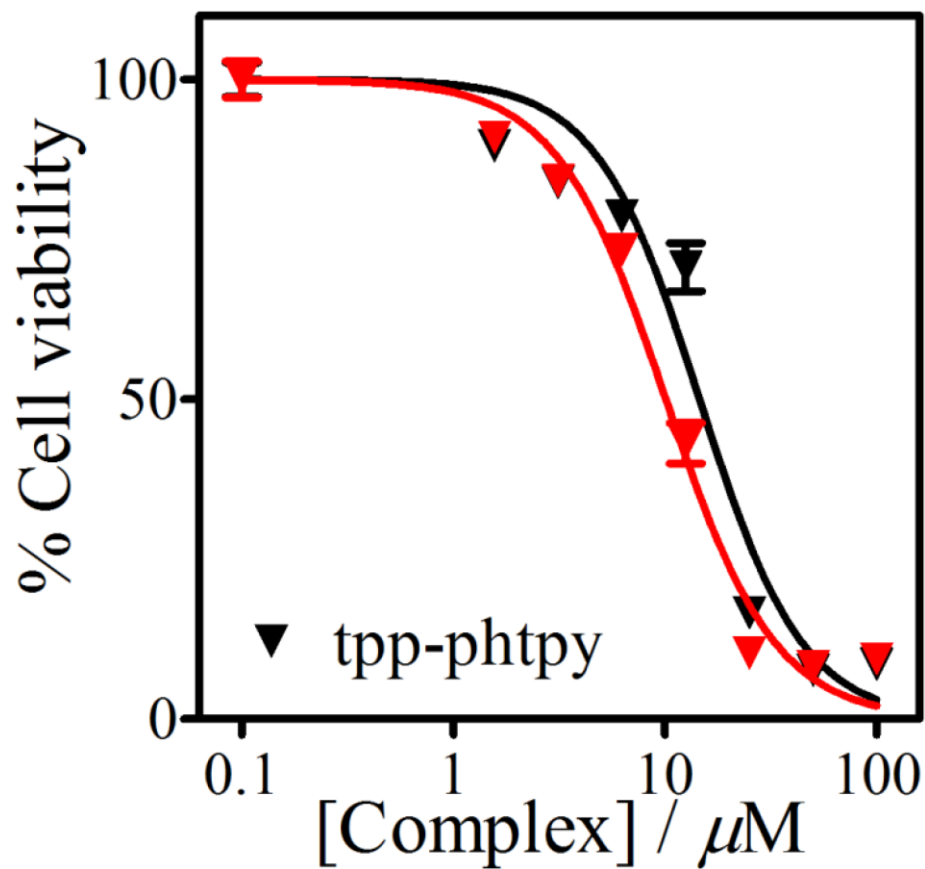


Fig. S11. Cell viability plots showing the cytotoxic effect of the TPP-phtpy ligand in dark (black symbols) and in visible light (red symbols, 400-700 nm, $10 J \text{ cm}^{-2}$) in HeLa cells.

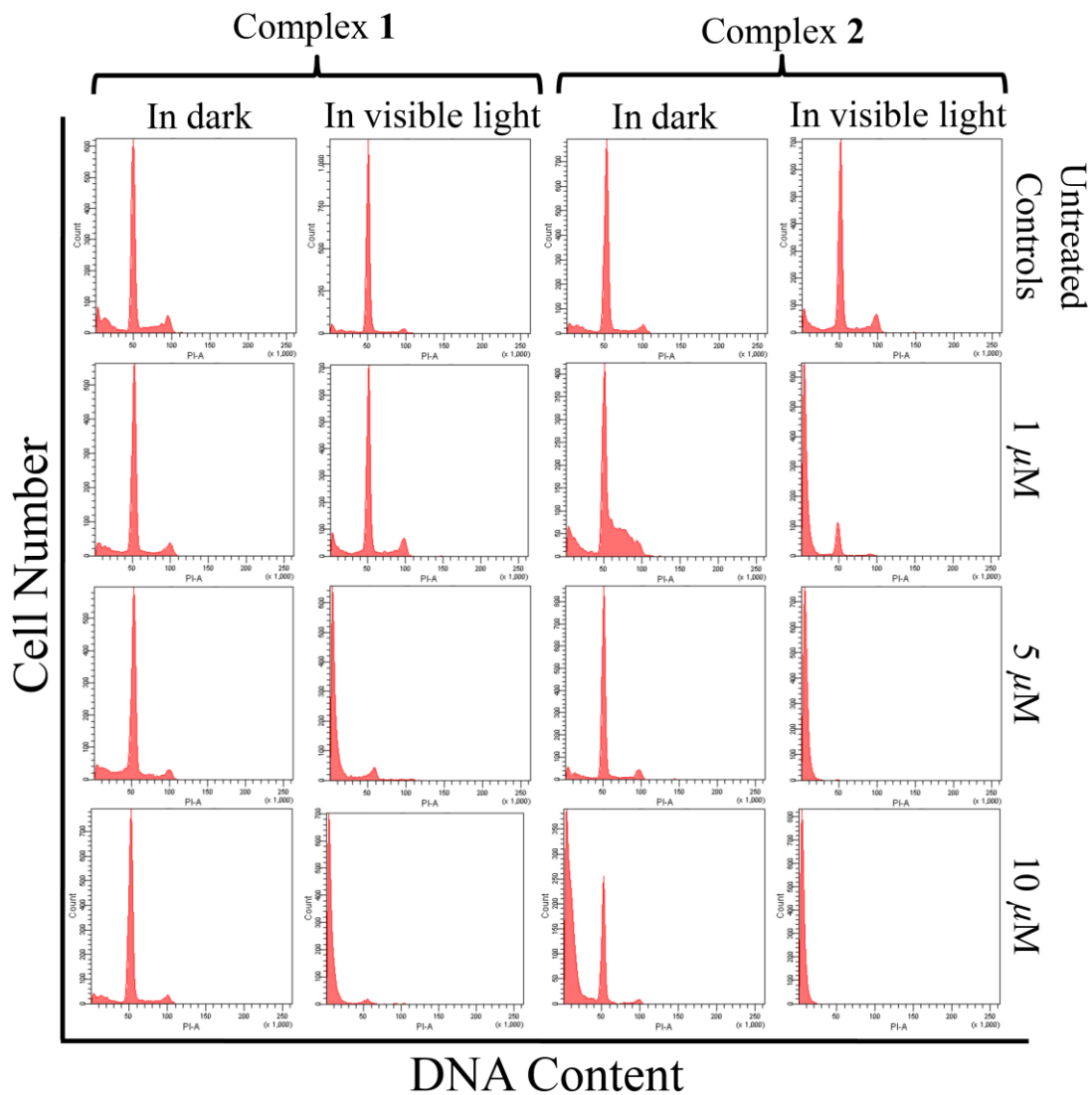


Fig. S12. Flow cytometric analysis of the apoptotic cell death induced by the curcumin complexes 1 and 2 in dark and on exposure to visible light (400-700 nm, 10 J cm^{-2}).

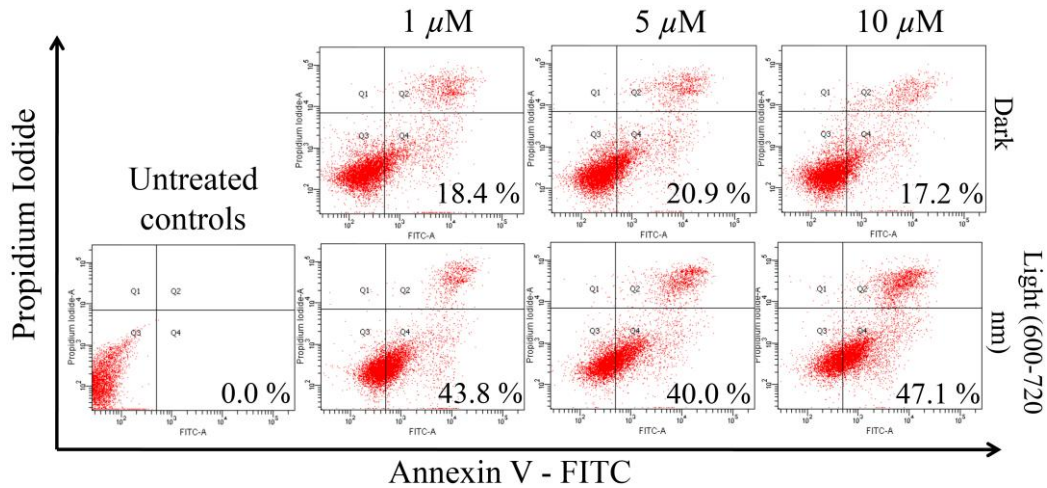


Fig. S13. Cellular apoptosis induced by complex **1** as determined from the annexin V-FITC/PI staining assay of the HeLa cells. Four distinct phenotypes: viable cells (lower left quadrant Q3); cells at an early stage of apoptosis (lower right quadrant Q4); cells at a late stage of apoptosis (upper right quadrant Q2); and necrosis (upper left quadrant Q1).

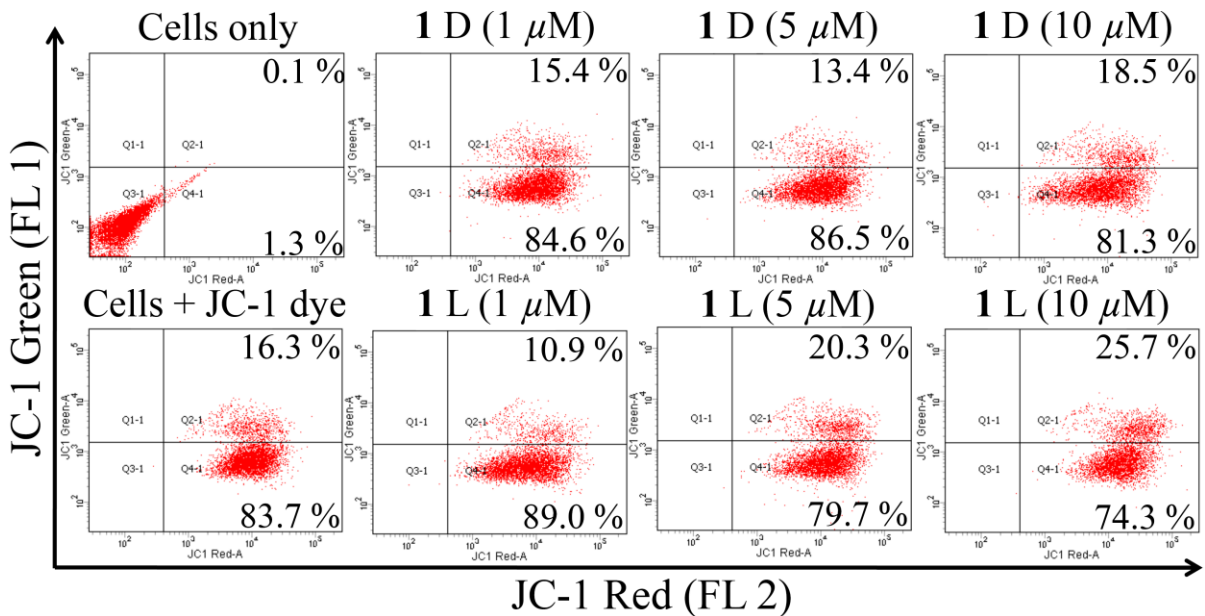


Fig. S14. Flow cytometric analysis (FACS) of the mitochondrial membrane potential using the JC-1 dye (20 nM) in HeLa cells treated with complex **1**. The % population of cells is given in the respective quadrants. D: dark; L: photo-irradiated with visible light (400–700 nm).

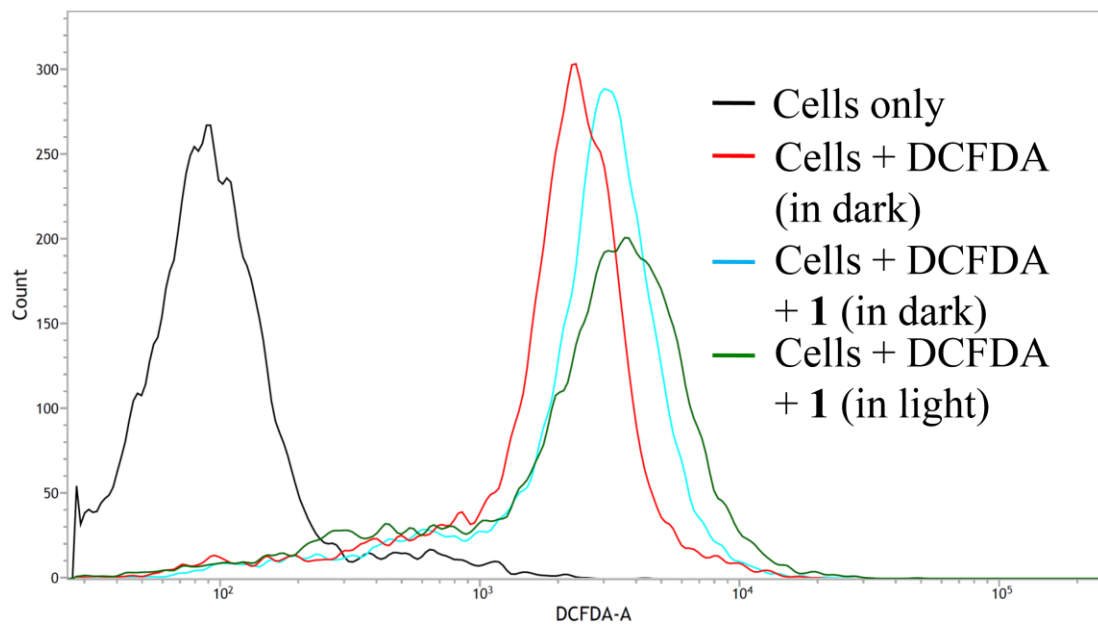


Fig. S15. Histogram showing the shift in the fluorescence intensity compared to that of only cells with addition of different additives as mentioned in the figure as determined by FACS studies. Greater shift implies higher fluorescence intensity resulting from higher amount of DCF formation and thus greater ROS generation.

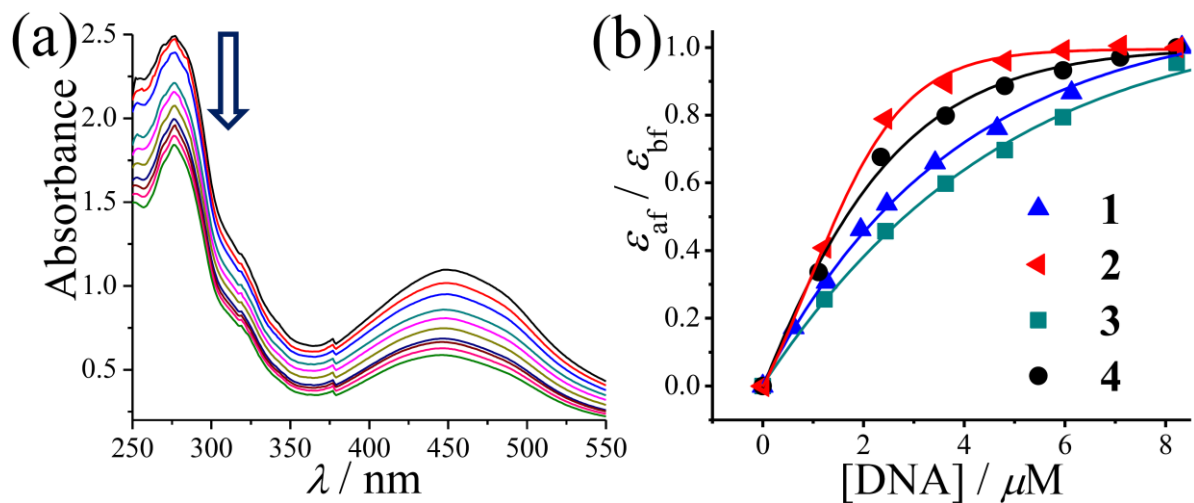


Fig. S16. (a) Absorption spectral traces of $[\text{VO}(\text{TPP-phtpy})(\text{cur})](\text{ClO}_4)$ (**2**) in 5 mM Tris-HCl buffer (pH 7.2) on increasing the quantity of ct-DNA (shown by arrow). (b) The least-squares fit of $\Delta\varepsilon_{\text{af}}/\Delta\varepsilon_{\text{bf}}$ vs. $[\text{DNA}]$ for the complexes $[\text{VO}(\text{phtpy})(\text{cur})](\text{ClO}_4)$ (**1**) (\blacktriangle), $[\text{VO}(\text{TPP-phtpy})(\text{cur})](\text{ClO}_4)$ (**2**) (\blacktriangleleft), $[\text{VO}(\text{phtpy})(\text{acac})](\text{ClO}_4)$ (**3**) (\blacksquare) and $[\text{VO}(\text{TPP-phtpy})(\text{acac})](\text{ClO}_4)$ (**4**) (\bullet).

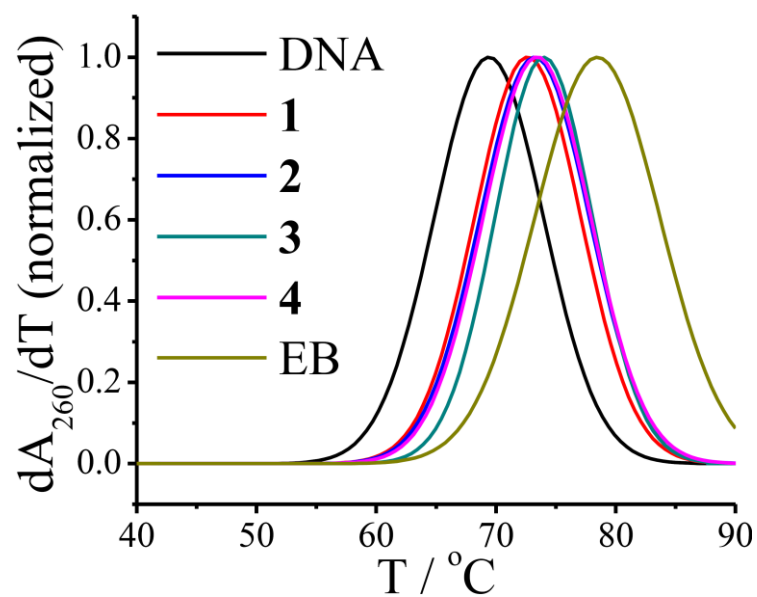


Fig. S17. Thermal denaturation plots of 150 μM ct-DNA alone and in the presence of the complexes **1-4** and ethidium bromide (EB) at $37.0(\pm 0.1)$ $^{\circ}\text{C}$ in 5 mM phosphate buffer (pH 6.85) with a [DNA]/[complex] ratio of 10:1.

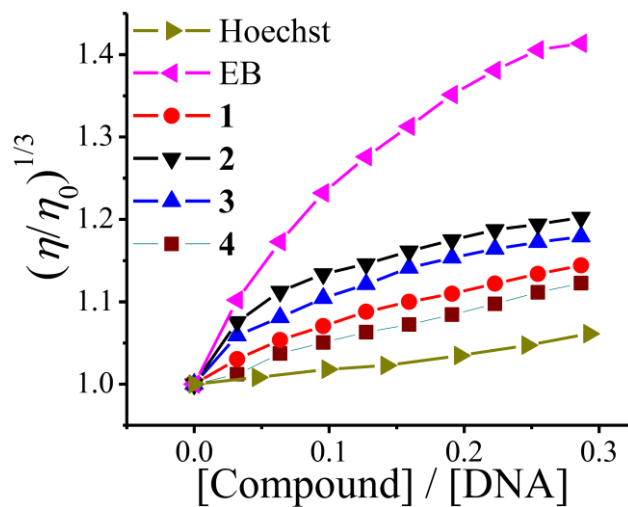


Fig. S18. Effect of increasing concentrations of the complexes **1 - 4**, EB and Hoechst 33258 on the relative viscosities of ct-DNA at $37.0(\pm 0.1)$ $^{\circ}\text{C}$ in 5 mmol Tris-HCl buffer (pH = 7.2, [DNA] = 150 μM).

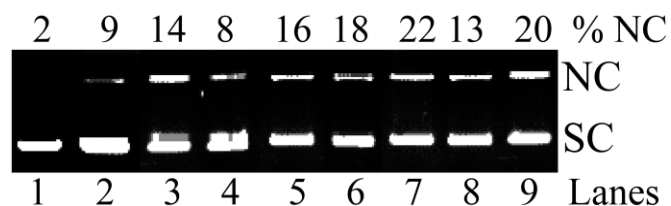


Fig. S19. Cleavage of SC pUC19 DNA (0.2 μg , 30 μM) by the complexes **1-4** and the ligands **in dark** in Tris-HCl buffer containing 10% DMF (complex concentration: 50 μM at 705 nm). lane 1, DNA control; lane 2, DNA + phtpy; lane 3, DNA + TPP-phpty; lane 4, DNA + Hacac, lane 5, DNA + Hcur; lane 6, DNA + **1**; lane 7, DNA + **2**, lane 8, DNA + **3**, lane 9, DNA + **4**.

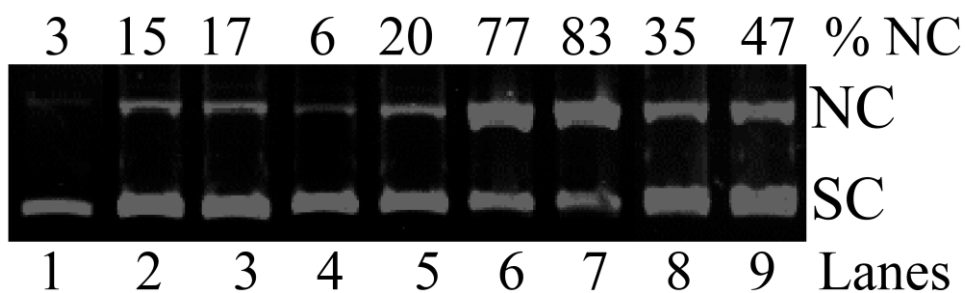


Fig. S20. Cleavage of SC pUC19 DNA (0.2 μg , 30 μM) by the complexes **1-4** and the ligands upon irradiation with **red light of 705 nm** for 2 h in Tris-HCl buffer containing 10% DMF (complex concentration: 50 μM at 705 nm). lane 1, DNA control; lane 2, DNA + phtpy; lane 3, DNA + TPP-phpty; lane 4, DNA + Hacac; lane 5, DNA + Hcur; lane 6, DNA + **1**; lane 7, DNA + **2**; lane 8, DNA + **3**; lane 9, DNA + **4**.

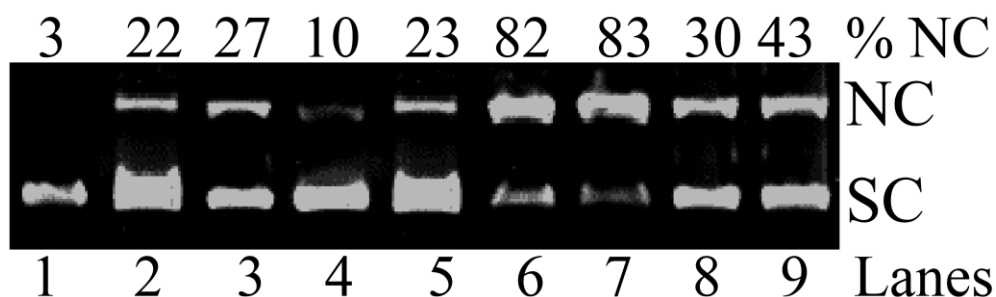


Fig. S21. Cleavage of SC pUC19 DNA (0.2 μg , 30 μM) by the complexes **1-4** and the ligands upon irradiation with **blue light of 454 nm** for 2 h in Tris-HCl buffer containing 10% DMF (complex concentration: 50 μM at 705 nm). lane 1, DNA control; lane 2, DNA + phtpy; lane 3, DNA + TPP-phpty; lane 4, DNA + Hacac; lane 5, DNA + Hcur; lane 6, DNA + **1**; lane 7, DNA + **2**; lane 8, DNA + **3**; lane 9, DNA + **4**.



Fig. S22. Cleavage of SC pUC19 DNA (0.2 μg , 30 μM) by [VO(phtpy)(cur)](ClO₄) (**2**) in the presence of various additives on irradiation with red light of 705 nm for 2 h in Tris-HCl buffer containing 10% DMF (complex concentration: 50 μM at 705 nm): lane 1, DNA control; lane 2, DNA + **2**; lane 3, DNA + **2** + NaN₃; lane 4, DNA + **2** + TEMP; lane 5, DNA + **2** + DABCO; lane 6, DNA + **2** + DMSO; lane 7, DNA + **2** + KI; lane 8, DNA + **2** + catalase.

